

Nanoscale Observation of Time-Dependent Domain Wall Pinning as the Origin of Polarization Fatigue

Sang Mo Yang, Tae Heon Kim, Jong-Gul Yoon, and Tae Won Noh*

The microscopic mechanism of polarization fatigue (i.e., a loss of switchable polarization under electrical cycling) remains one of the most important long-standing problems in ferroelectric communities. Although there are numerous proposed fatigue models, a consensus between the models and experimental results is not reached yet. By using modified-piezoresponse force microscopy, nanoscale domain switching dynamics are visualized for different fatigue stages in epitaxial $\text{PbZr}_{0.4}\text{Ti}_{0.6}\text{O}_3$ capacitors. Systematic time-dependent studies of the domain nucleation and evolution reveal that domain wall pinning, rather than nucleation inhibition, is the primary origin of fatigue. In particular, the evolution of domain wall pinning process during electrical cycling, from the suppression of sideways domain growth in early fatigued stages to the blockage of forward domain growth in later stages, is directly observed. The pinning of forward growth results in a nucleation-limited polarization switching and a significant slowdown of the switching time in the severely fatigued samples. The direct nanoscale observation of domain nucleation and growth dynamics elucidates the importance of evolution of the domain wall pinning process in the fatigue of ferroelectric materials.

hindrance restricting the reliability of FE-based devices.

Since the fatigue phenomenon was reported by Merz and Anderson as early as 1955,^[10] a flurry of studies has followed, especially during the last two decades.^[8,9,11–26] Despite such extensive efforts, the microscopic mechanism of polarization fatigue is still controversial and remains an important long-standing problem in FE materials. Many fatigue models have been proposed, including the formation of extended defects capable of domain wall pinning,^[3,15–17] nucleation inhibition induced by charge injection,^[8,18] growth of a nearby electrode non-switching/dead layer,^[19,20] and local phase decomposition.^[9,21] However, no model can provide answers to all questions related how the fatigue starts and evolves with electrical cycling.

The proposed fatigue models are generally based on the following two-step sce-

1. Introduction

Ferroelectric (FE) materials are fascinating and practical because of the spontaneous polarization, which is strongly coupled to long-range electric and stress fields, leading to outstanding properties such as switchability of electrical polarization and piezoelectricity.^[1–3] Thus, based on those captivating properties, it has been numerous efforts to develop the advanced FE-based electronic devices, including FE random access memories,^[3] field-effect transistors,^[4] and recently FE tunneling junctions.^[5–7] However, there are several obstacles to the realization of high-performance devices. One prime example is the fatigue problem. Polarization fatigue is a loss of switchable polarization under bipolar electrical cycling.^[3,8,9] It has posed a critical

scenario: i) applied electrical cycling results in the creation and/or redistribution of charged defects in FE materials and ii) such defects influence FE domain switching process, leading to a loss of switchable polarization.^[8] Some researchers have suggested that oxygen vacancies act as charged defects,^[3,14–17] but others have claimed that trapped electronic charges play an important role.^[8,18,22] Depending on the identities of the defects and their collective behaviors, each fatigue model suggests a different FE domain switching process.^[8] For example, the embryonic nucleation sites are prohibited from occurring nucleation process (i.e., nucleation inhibition)^[8,18] or the domain walls do not propagate any longer due to pinning (i.e., domain wall pinning).^[3,15–17] Therefore, to elucidate the microscopic fatigue mechanism, it is imperative to look directly into changes in domain switching process under electrical cycling. Nevertheless, there has been no direct observation of how domain nucleation and growth dynamics actually change in time (i.e., electrical cycling) at the same sample position in real capacitor geometry.

It should be noted that FE domain switching typically occurs over a length scale ranging from nanometers to micrometers, with associated time scale from nanoseconds to milliseconds or longer.^[3,27] Many researchers have used macroscopic (i.e., spatially averaged) probing tools, such as polarization–electric field (P – E) hysteresis loops.^[3,8,9] However, those studies have not been able to provide the information on the domain dynamics

S. M. Yang, T. H. Kim, Prof. T. W. Noh
Research Center for Functional Interfaces
Department of Physics and Astronomy
Seoul National University
Seoul 151-747, Korea
E-mail: twnoh@snu.ac.kr

Prof. J.-G. Yoon
Department of Physics
University of Suwon
Hwaseong, Gyeonggi-do 445-743, Korea



DOI: 10.1002/adfm.201102685

under fatigue. To obtain nanoscale pictures on fatigue, some researchers have used conventional piezoresponse force microscopy (PFM).^[23–25,28,29] Although this method can provide microscopic pictures, they had to speculate on the domain dynamics from static PFM images. Up to this point, there have been few efforts to carry out direct investigations of time (t)-dependent nanoscale FE domain switching dynamics during fatigue.^[13] The main reason is that it is experimentally difficult to simultaneously cover such wide time and length scales, when FE domain switching is in progress.

Here, we present a nanoscale investigation of how the FE domain switching process varies with electrical cycling in epitaxial $\text{PbZr}_{0.4}\text{Ti}_{0.6}\text{O}_3$ (PZT) capacitors. We visualized the FE domain nucleation and growth for different fatigue stages using modified-PFM. The modified-PFM has significant advantages for investigating t -dependent domain dynamics, such as defect-mediated nucleation^[30] and domain wall motion.^[31–33] Using this technique, we found that domain wall pinning, rather than nucleation inhibition, is the primary origin of polarization fatigue in epitaxial PZT films. In addition, we discovered that sideways domain wall motion becomes suppressed in the early fatigued stages but forward domain growth becomes blocked in the later stages. This finding on the time-dependent domain wall pinning process makes additional important advances towards a complete understanding of polarization fatigue in FE thin films.

2. Results and Discussion

2.1. Hysteresis Loops and Switching Current Measurements

For this study, we used high-quality Au/PZT/SrRuO_3 capacitors grown on SrTiO_3 (001) substrates as a model system.^[30] Our PZT capacitors showed a characteristic fatigue behavior as electrical cycling proceeded. Figure 1a shows P - E hysteresis loops of a PZT capacitor for virgin and various fatigued states. The P - E hysteresis loop for the virgin state was nearly square, indicating the high FE quality of our PZT capacitors. To obtain the fatigued states, we applied 5- μs -wide bipolar pulses with a frequency of 100 kHz. The hysteresis loops became slanted as the number of cycles increased, and a reduction in remnant polarization ($2P_r$) was observed, as reported in other fatigue studies.^[3,8,9] The virgin state of $2P_r \approx 100 \mu\text{C cm}^{-2}$ began to degrade after 10^3 cycles and was reduced to $\approx 45 \mu\text{C cm}^{-2}$ after 10^5 cycles, showing the progress of the fatigue in the PZT capacitors (Figure 1b).

As fatigue proceeded, the macroscopically observed domain switching process slowed significantly. By measuring the transient switching currents (Supporting Information), we determined switchable polarization $\Delta P(t)$, the extent to which P reversed in time. Figure 1c shows $\Delta P(t)$ of the PZT capacitor under -150 kV cm^{-1} after various electrical cycles. With increasing cycles, ΔP was reduced, in agreement with the $2P_r$ values of the P - E hysteresis loop measurements. Additionally, the full-switching time, when ΔP value becomes saturated, slowed significantly.^[34] These observations suggest that the average P switching time increases drastically as a result of

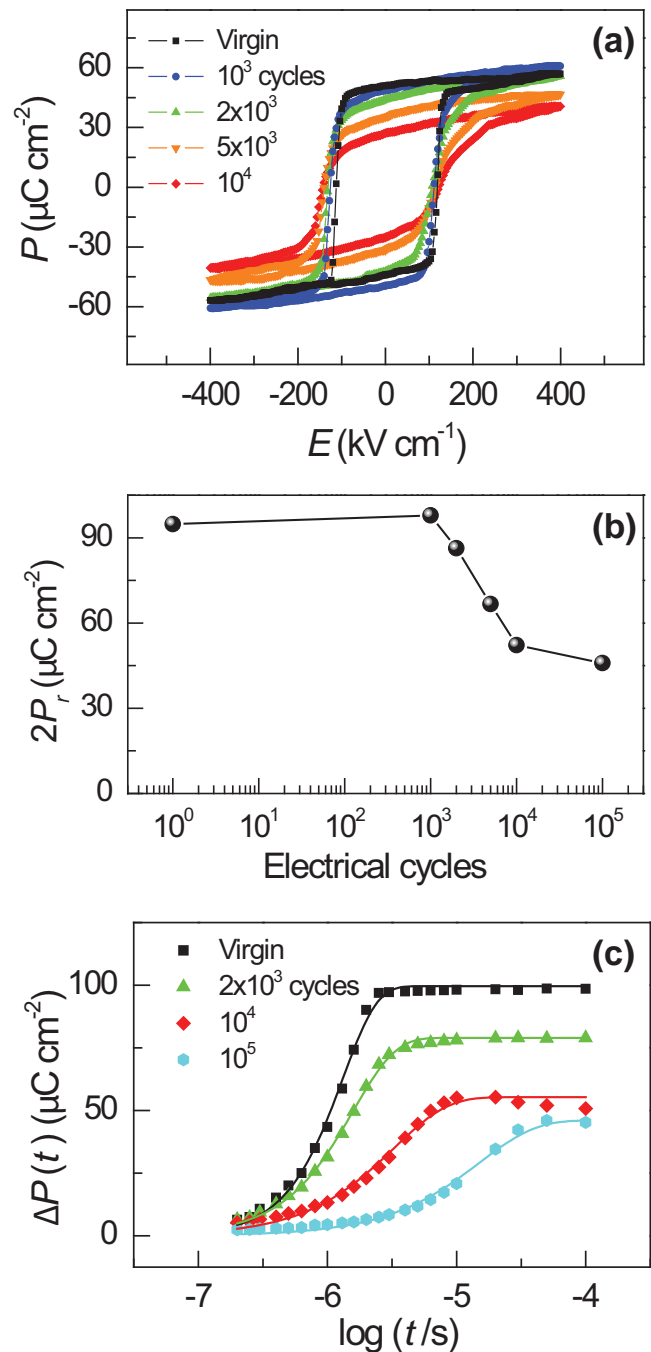


Figure 1. a) P - E hysteresis loops of the PZT capacitor for the virgin and various fatigued states. b) Remnant polarization ($2P_r$) as a function of electrical cycles. c) Time (t)-dependent switchable polarization ($\Delta P(t)$) of the PZT capacitor under -150 kV cm^{-1} after various electrical cycles. The solid lines indicate the fitting lines based on the KAI model.

fatigue. However, these spatially averaged data do not provide the essential nanoscale information of domain dynamics under fatigue. It should be clarified how such a slowdown occurs among the various steps of the domain switching process, i.e., nucleation, forward growth, and/or sideways growth of domains.

2.2. Imaging of Time-Dependent Domain Dynamics During Fatigue

To investigate how electrical cycling affects the evolution of nanoscale FE domain dynamics, we measured t -dependent PFM images for virgin and fatigued PZT capacitors. We used the domain-tracing method to obtain consecutive PFM images over time.^[27,31] We initially poled the capacitors using a pulsed field ($+400 \text{ kV cm}^{-1}$, $200 \mu\text{s}$) and then successively applied the switching pulsed fields of -150 kV cm^{-1} . We measured the PFM images between the switching pulsed fields.

Note that we can obtain two kinds of PFM images. One is the phase image, which indicates the spatial distribution of the P direction. For instance, in the phase images of **Figure 2a**, the bright yellow regions display the nucleated and grown domains with upward P (pointing towards the top electrode), while the dark brown regions show downward P domains. The other is the amplitude image, which shows the spatial distribution of the piezoresponse magnitude. As shown in the amplitude images of **Figure 2a**, the dark blue lines indicate the domain

walls, around which the local piezoresponse nearly vanishes. Details of the contrast change in the phase and amplitude images are described in **Figure S2** of Supporting Information.

Figure 2a shows t -dependent FE domain evolution in a virgin capacitor. An electric field was applied opposite to the initial P direction. Most of the nucleation process occurred at a total pulse width of $t = 0.5 \mu\text{s}$ or less, and then those nucleated domains expanded sideways. At $t = 2.0 \mu\text{s}$ or above, most of the domains coalesced to form a large FE domain with opposite P . In the corresponding amplitude images, we also observed the propagation of domain walls. In the conventional picture, FE domain switching should occur through the nucleation of domains with opposite P , followed by their forward growth across the film and sideways motion of the domain walls^[3,27,35,36] (Supporting Information, **Figure S2**). Therefore, the domain evolution observed in the virgin capacitor is consistent with the conventional picture of FE domain switching.

In contrast, the fatigued capacitor shows the different domain switching behavior, which cannot be explained by the conventional FE domain switching picture. **Figure 2b** shows

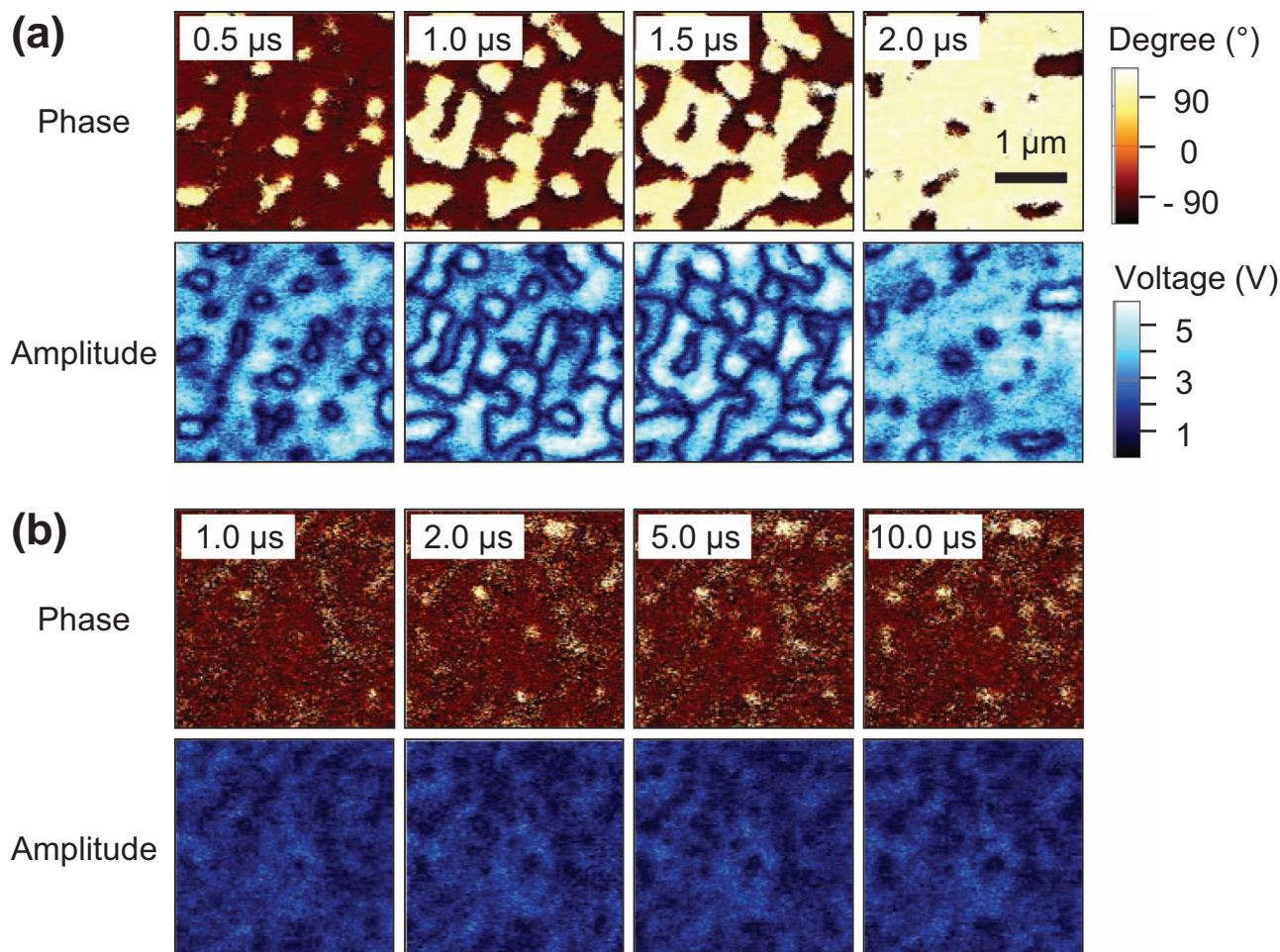


Figure 2. Time-dependent PFM phase and amplitude images of domain evolution under -150 kV cm^{-1} for a) the virgin state and b) the fatigued state (after 10^4 cycles). The time indicates the total width of the applied switching pulses. The scan area was $3 \times 3 \mu\text{m}^2$. All images were measured at the same sample position.

the t -dependent FE domain evolution after 10^4 cycles. Although the PFM images in Figure 2a,b were taken at the same sample position, they appeared to be significantly different. Particularly, for the fatigue sample, the reversed domains were nanosized and spot-like. But most regions retained the initial downward P , called unswitchable frozen domain regions.^[23–25] The images looked similar to the Milky Way. Nucleation appeared to occur continuously. However, most nucleated domains did not grow laterally and sustained their sizes and shapes, indicating that the domain walls were pinned. We measured the sideways domain wall velocity v directly as a function of electrical cycling (Supporting Information, Figure S3). The v value decreased with increasing cycles and finally approached zero for the severely fatigued states (after 5×10^3 cycles in this study). All of these experimental observations indicate that the sideways domain wall motion became suppressed significantly due to domain wall pinning.

It is important to note that the contrast of the amplitude images of the fatigued state (Figure 2b), was much darker over the entire scan area than that of the virgin state (Figure 2a). This indicates that the piezoresponse magnitude of a given site decreased considerably with electrical cycling. Recently, Murari et al. reported a uniform decrease in the piezoresponse under fatigue in epitaxial $\text{PbZr}_{0.2}\text{Ti}_{0.8}\text{O}_3$ films using the second harmonic PFM technique.^[37] Interestingly, we further observed that the piezoresponse of the regions corresponding to nanosized reversed domains (i.e., bright yellow domains in the phase image) was smaller than that of other regions. This can be interpreted in terms of incomplete forward domain growth. Namely, if the forward domain growth is not complete, the contributions from the upward and downward P domains to piezoresponse may have cancelled each other, causing an additional decrease in amplitude signal. This implies that most nucleated domains in the severely fatigued samples should experience incomplete forward domain growth.

2.3. Imaging of Nucleation Process During Fatigue

The repetitive electrical cycling should also strongly affect the nucleation process. In most real FE systems, nucleation usually occurs at particular sites; this is known as inhomogeneous nucleation.^[27,30,38] Thus, the nucleation sites can be visualized by summing many PFM images at the same sample position.^[30] Figure 3a–c shows the nucleation sites for the virgin state, after 2×10^3 cycles, and 5×10^3 cycles, respectively. The dashed open white circles indicate the nucleation sites that emerged for all states, suggesting inhomogeneous nucleation. Note that in Figure 3b,c, some nucleation sites in the virgin state disappeared after electrical cycling, indicating the nucleation inhibition sites (open red diamonds). Additionally, such nucleation inhibition sites increased with electrical cycling. However, it should be noted that several additional nucleation sites were also observed in Figure 3b,c. Furthermore, we observed that specific nucleation sites varied as fatigue proceeded, even within the same dashed open white circles.

According to the nucleation inhibition model, one of major fatigue mechanisms, electrical cycling injects electronic charges into the FE samples and blocks the nucleation seeds.^[8,18] These

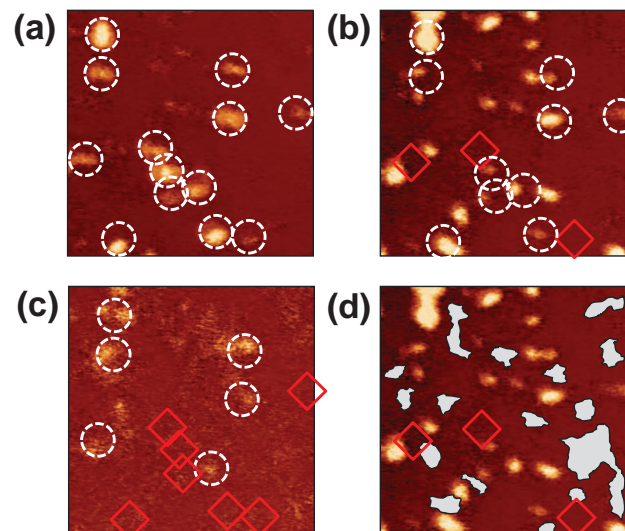


Figure 3. Nucleation sites a) for the virgin state, b) after 2×10^3 cycles, and c) after 5×10^3 cycles obtained by summing ten PFM phase images at the same sample position. The scan area was $3 \times 3 \mu\text{m}^2$. The dashed open white circles indicate the nucleation sites that emerged for all states. The open red diamonds show the nucleation inhibition sites, which did not appear for each fatigued state. d) Direct comparison between the frozen domain regions (solid gray regions) and the nucleation inhibition sites (open red diamonds) after 2×10^3 cycles.

nucleation inhibition sites in their embryonic state do not allow domain switching any longer; thus, the unswitchable frozen domain regions should correspond to nucleation inhibition sites.^[8,18] To check the validity of the nucleation inhibition model, we compared the nucleation sites with the frozen domain regions. The frozen domain regions for the fatigued capacitor (after 2×10^3 cycles) are represented by the gray regions in Figure 3d. Additionally, we overlaid the nucleation inhibition sites (open red diamonds). It is clear that the frozen domain regions do not coincide with the nucleation inhibition sites, indicating that the nucleation inhibition model cannot be applicable to the fatigue of epitaxial FE thin films (also see Supporting Information, Figure S6).

2.4. Evolution of Domain Wall Pinning Process

We further compared our experimental results with predictions by the domain wall pinning mechanism.^[3,15–17] In spite of the extensive efforts expended on this mechanism, there is still considerable room for improvement. For example, it is not still established whether domain wall pinning occurs during forward or sideways domain growth.^[15] In addition, it is not known how the detailed domain wall pinning process changes with electrical cycling. Here, we will address these essential issues using the modified PFM to develop a complete understanding of polarization fatigue.

By combing the PFM amplitude and phase images, we can distinguish the forward growth from the sideways growth of FE domains.^[39] Figure 4a shows a schematic diagram of the cross-section of the FE capacitor, which displays a domain experiencing the forward growth (Type A) and sideways growth (Type

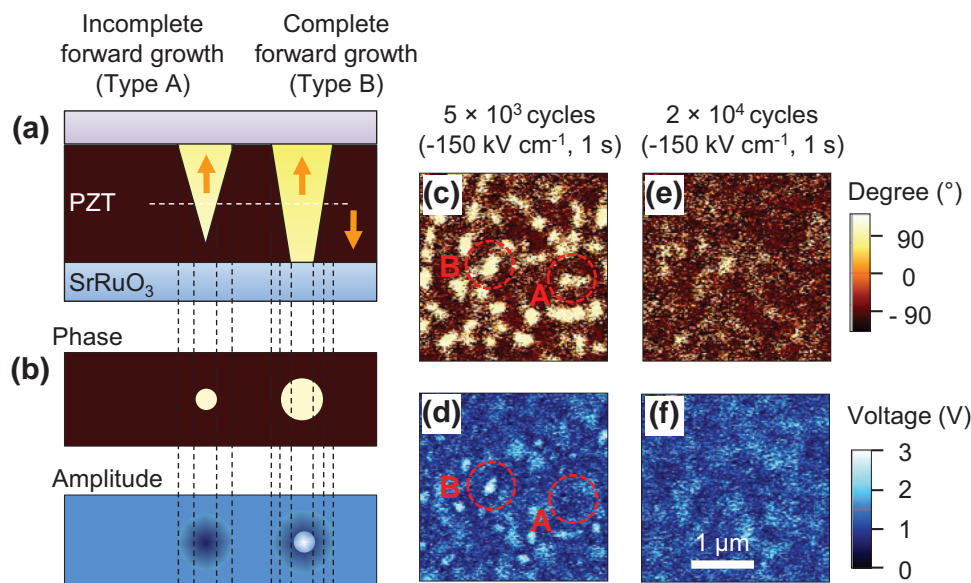


Figure 4. a) Schematic diagram of the cross-section of the PZT capacitor, showing the incomplete and complete forward domain growths. The arrows indicate the polarization direction of the domains. b) Predicted PFM top-view images of phase and amplitude signals corresponding to each type. Measured PFM phase (c,e) and amplitude (d,f) images under -150 kV cm^{-1} with $t = 1 \text{ s}$ after 5×10^3 cycles and 2×10^4 cycles, respectively.

B). The corresponding predicted PFM top-view images of phase and amplitude signals are shown in Figure 4b. When the forward domain growth was incomplete, as in Type A, the amplitude signal was reduced in the reversed domain regions, and the phase signal changed only in the regions with more than 50% reversal across the film (see Supporting Information, Figure S2). On the other hand, when the forward growth was complete and the sideways growth was in progress, as in Type B, the amplitude signal had a doughnut shape with a bright core (large piezoresponse) and dark circumference (small piezoresponse).

Figure 4c,d show the phase and amplitude images, respectively, of a fatigued PZT capacitor with $E = -150 \text{ kV cm}^{-1}$ and $t = 1 \text{ s}$ after 5×10^3 cycles. Note that, in Figure 4d, most reversed domains are Type A and the doughnut shape of Type B can be observed for only several reversed domains. Considering that forward domain growth is typically complete within 1 ns for films that are a few micrometers thick,^[3] it is reasonable to conclude that the forward growth was blocked in Type A. Thus, we conclude that not only the sideways domain wall motion but also the forward domain growth was pinned for the severely fatigued states. Additionally, Figure 4e,f shows PFM images after 2×10^4 cycles, i.e., for a more fatigued sample. It is clear that nearly all of the forward growth became blocked. This indicates that the dominant domain wall pinning process evolved from the suppression of sideways domain wall motion (in the early fatigued stages) to blockage of forward growth (in the severely fatigued stages).

2.5. Interpretation of Switching Current Measurement Results

The evolution of the domain wall pinning process should result in changes in the macroscopic physical properties. To verify this, we fitted the switching current data in Figure 1c with the Komogorov–Avrami–Ishibashi (KAI) model (Supporting Information).^[40] The KAI model gives $\Delta P(t)$ as

$$\Delta P(t) = 2P_1[1 - \exp\{-(t/t_0)^n\}], \quad (1)$$

where t_0 is the characteristic switching time. And n is related to an effective dimension of the domain growth d .^[40] As displayed by the solid lines in Figure 1c, the fitting results agreed with the experimental data. Table 1 shows the values of t_0 and n for virgin and various fatigued states. Note that characteristic switching time t_0 values increase with electrical cycling. As the fatigue proceeds, the amount of domain wall pinning effectively increases, which results in the slowdown of t_0 .

The change in the dominant domain wall pinning process is also reflected in the effective domain growth dimension d . In Table 1, the n value changes from 1.66 for the virgin state to nearly 1.0 for the severely fatigued states. When all nuclei are generated instantaneously, n should correspond to d .^[40] In the virgin state, most nuclei are generated during the initial stage and most P switching is accomplished via forward and sideways growth rather than nucleation. So we can conclude that $n = d$ for the virgin state. Therefore, the n value of 1.66 indicates that most nucleated domains grew either one- or two-dimensionally.^[41]

On the other hand, in the fatigued state, P switching via forward and sideways growth becomes nearly impossible due to

Table 1. The values of t_0 and n based on the KAI model fitting to the switching current data (Figure 1c) for the virgin and various fatigued states.

Electrical cycles	t_0 [s]	n
virgin	1.30×10^{-6}	1.66
2×10^3	1.59×10^{-6}	1.33
10^4	3.27×10^{-6}	1.05
10^5	1.50×10^{-5}	0.99

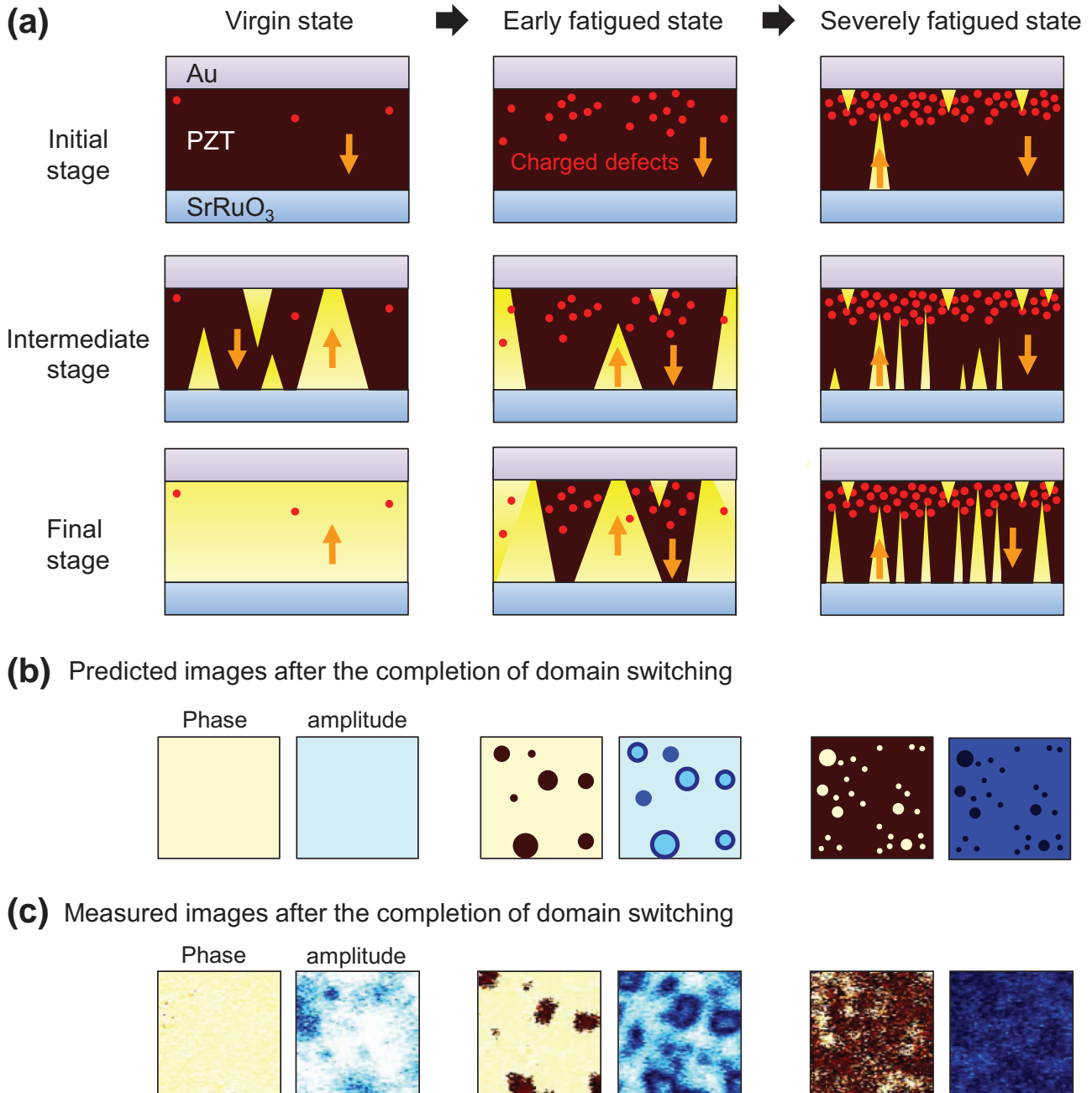


Figure 5. a) Schematic diagrams of the cross-section of the PZT capacitor showing the time-dependent domain switching process for the different fatigued states. The arrows indicate the polarization direction of the domains. The small red dots show the charged defects, which can pin domain walls. The b) predicted and c) measured PFM (top-view) phase and amplitude images after the completion of domain switching for each states.

domain wall pinning. Thus, P switching should be limited by nucleation. When the nuclei are generated at a constant rate, as in the nucleation-limited switching, n should correspond to $d + 1$.^[40] Therefore, the value of $n \approx 1.0$ from the KAI fitting can be interpreted as the continuously nucleated domains not being able to grow further, i.e., $d = 0$. This argument is consistent with the observed PFM images, showing that for the severely fatigued states the domain switching was primarily due to the generation of spot-like domains, not forward and sideways growth of nucleated domains.

2.6. Proposal of Time-Dependent Domain Wall Pinning Mechanism

Adopting this nanoscale dynamic information, we propose a time-dependent domain wall pinning mechanism, which contains the blockage of forward and sideways domain growth in detail. A schematic illustration is shown in **Figure 5a**. Note that we assumed initial monodomain states with downward P , as indicated by the arrows. The small red dots indicate the charged defects in FE materials, which can be created and migrated by

an applied electric field. We suggest that oxygen vacancies are a strong candidate for such defects. Many researchers have reported that oxygen vacancies preferentially electromigrate to the electrode/FE interfaces and form extended defects.^[3,15–17] Under electrical cycling, oxygen vacancies are likely to be generated mostly near the Au/FE top interface. However, there would be few oxygen vacancies near the FE/SrRuO₃ bottom interface because oxygen is supplied from the SrRuO₃ oxide electrode.

The density of charged defects and their spatial distribution determine the evolution of the domain wall pinning process during fatigue. Figure 5a displays the *t*-dependent domain switching process for the different fatigued states: the first column for the virgin state, the second column for the early fatigued state, and the final column for the severely fatigued state. For the virgin state, there are few defects that can pin domain walls. Thus, the FE domains can be switched freely by an external electric field via the aforementioned conventional domain switching process. For the early fatigued state, charged defects such as oxygen vacancies will migrate near to the Au/FE interface and form extended defects.^[3,15–17] The density of extended defects is relatively low. Unless the nucleated domains meet with such defect clusters, they can complete the forward growth and continue the subsequent sideways domain wall motion. If the domain wall pinning occurs due to defect clusters during sideways growth, frozen domain regions will appear. Finally, as electrical cycling proceeds, the number of extended defects increases considerably. For the severely fatigued states, they can distribute widely over the entire sample like a plane (such a defect plane might be interpreted as a nonswitching/dead layer).^[19,20] These concentrated defects play an important role in blocking the forward growth of nucleated domains.

The predicted PFM images after the completion of domain switching at each state are shown in Figure 5b. For the virgin state, when the domain switching is complete, a monodomain with upward *P* is predicted. For the early fatigued state, most domain wall pinning occurs during sideways growth, so the PFM images should show the frozen domain regions, as shown in the second set of the PFM images. For the severely fatigued state, most forward domain growth becomes blocked. Thus, the PFM should show many nanosized and spot-like domains, as shown in the third set of the PFM images. Additionally, the existence of widely distributed defect clusters causes a uniform decrease in the amplitude signal, and the blocking of forward growth induces an additional decrease in the amplitude signal. Note that all of these predicted PFM images in Figure 5b are in good agreement with the measured PFM images, as shown in Figure 5c. This demonstrates the validity of our proposed model as a fatigue mechanism.

3. Conclusions

In summary, we investigated how nanoscale FE domain dynamics in epitaxial PZT capacitors become evolved during fatigue. By using modified-PFM, we studied nanoscale FE domain nucleation, subsequent forward growth, and sideways domain wall motion for various fatigue states (namely in virgin, early fatigued, and severely fatigued samples). The severely fatigued samples showed dense domain structures composed of many nanosized spot-like domains, which cannot grow further

due to surrounding frozen domain regions. The obtained nanoscale dynamic information revealed clearly that domain wall pinning, rather than nucleation inhibition, is the primary origin of polarization fatigue in epitaxial FE films. Furthermore, we found that the dominant domain wall pinning process changed from the suppression of sideways growth in the early fatigued states to the blockage of forward growth in the severely fatigued states. This direct nanoscale observation of domain nucleation and growth processes provides a comprehensive understanding of polarization fatigue in FE materials.

4. Experimental Section

Materials: High-quality Au/PbZr_{0.4}Ti_{0.6}O₃ (PZT)/SrRuO₃ capacitors grown on SrTiO₃ (001) substrates were used as a model system. The PZT films were deposited on SrRuO₃/SrTiO₃ (001) using pulsed laser deposition.^[30] High-resolution X-ray diffraction studies confirmed that the PZT films were epitaxial with purely *c*-axis-oriented domains, implying that only 180° domain walls should exist.^[30] This epitaxial PZT system was chosen to provide a sample with a simple domain switching path. Compared to films with various switching paths, such as rhombohedral BiFeO₃ (001) films (three possible switching paths),^[14] the tetragonal PZT (001) films have only one domain switching path from upward polarization to downward polarization and vice versa (i.e., 180° domain switching). Additionally, the extrinsic effects on the ferroelectric domain switching process due to the microstructure of the sample were minimized. Compared to polycrystalline films, the epitaxial films are not affected by grain boundaries and grains with different crystallographic orientations. To observe fatigue behavior, Au top electrodes with a diameter of 100 μm were deposited by sputtering with a shadow mask. Note that fatigue behavior was not observed up to 10¹⁰ cycles in the SrRuO₃/PZT/SrRuO₃ capacitors.^[30] The thicknesses of the PZT films and Au top electrodes were 200 and 40 nm, respectively.

Experimental Setup: Modified-piezoresponse force microscopy (PFM) was developed based on a commercial system (XE-100, Park systems).^[27,30] In this setup, due to additional probe needle,^[27,30] other electrical measurements could also be performed, including transient switching current measurements and polarization-electric field (*P*–*E*) hysteresis loop measurements, as well as PFM imaging. For the PFM imaging, the ac voltage of 0.2 V_{rms} at 19.1 kHz was directly applied to the additional probe needle. Additionally, an arbitrary wave form generator (FG300, Yokogawa) and a lock-in amplifier (SR830, Stanford Research Systems) were used. The cantilever was the non-conductive silicon cantilever (FORTA, Appnano). For the switching current measurements, the aforementioned arbitrary wave form generator and a digital oscilloscope (DL7100, Yokogawa) were used. The *P*–*E* hysteresis loop measurements were performed using a TF analyzer 2000 (aixACCT). For data analysis, the WSxM program^[42] and XEI program (Park systems) were used.

Supporting Information

Supporting Information is available from the Wiley Online Library or from the author.

Acknowledgements

S.M.Y. thanks Dr. D. J. Kim and Dr. B. Chen for their help. This work was supported by the National Research Foundation (NRF) of Korea grant funded by the Ministry of Education, Science and Technology (MEST) (Grant No. 2010-0020416).

Received: November 8, 2011
Published online: March 14, 2012

- [1] C. H. Ahn, K. M. Rabe, J. M. Triscone, *Science* **2004**, *303*, 488.
- [2] M. E. Lines, A. M. Glass, *Principles and Applications of Ferroelectrics and Related Materials*, Clarendon Press, Oxford **1977**.
- [3] J. F. Scott, *Ferroelectric memories*, Springer, Berlin **2000**.
- [4] S. Mathews, R. Ramesh, T. Venkatesan, J. Benedetto, *Science* **1997**, *276*, 238.
- [5] V. Garcia, S. Fusil, K. Bouzehouane, S. Enouz-Vedrenne, N. D. Mathur, A. Barthelemy, M. Bibes, *Nature* **2009**, *460*, 81.
- [6] A. Gruverman, D. Wu, H. Lu, Y. Wang, H. W. Jang, C. M. Folkman, M. Y. Zhuravlev, D. Felker, M. Rzchowski, C. B. Eom, E. Y. Tsymlal, *Nano Lett.* **2009**, *9*, 3539.
- [7] P. Maksymovych, S. Jesse, P. Yu, R. Ramesh, A. P. Baddorf, S. V. Kalinin, *Science* **2009**, *324*, 1421.
- [8] A. K. Tagantsev, I. Stolichnov, E. L. Colla, N. Setter, *J. Appl. Phys.* **2001**, *90*, 1387.
- [9] X. J. Lou, *J. Appl. Phys.* **2009**, *105*, 024101.
- [10] W. J. Merz, J. R. Anderson, *Bell Lab. Rec.* **1955**, *33*, 335.
- [11] B. H. Park, B. S. Kang, S. D. Bu, T. W. Noh, J. Lee, W. Jo, *Nature* **1999**, *401*, 682.
- [12] C. A. P. de Araujo, J. D. Cuchiaro, L. D. McMillan, M. C. Scott, J. F. Scott, *Nature* **1995**, *374*, 627.
- [13] D.-H. Do, P. G. Evans, E. D. Isaacs, D. M. Kim, C. B. Eom, E. M. Dufresne, *Nat. Mater.* **2004**, *3*, 365.
- [14] S.-H. Baek, C. M. Folkman, J.-W. Park, S. Lee, C.-W. Bark, T. Tybell, C.-B. Eom, *Adv. Mater.* **2011**, *23*, 1621.
- [15] J. F. Scott, M. Dawber, *Appl. Phys. Lett.* **2000**, *76*, 3801.
- [16] M. Dawber, J. F. Scott, *Appl. Phys. Lett.* **2000**, *76*, 1060.
- [17] C. Brennan, *Ferroelectrics* **1993**, *150*, 199.
- [18] E. L. Colla, D. V. Taylor, A. K. Tagantsev, N. Setter, *Appl. Phys. Lett.* **1998**, *72*, 2478.
- [19] A. M. Bratkovsky, A. P. Levanyuk, *Phys. Rev. Lett.* **2000**, *84*, 3177.
- [20] P. K. Larsen, G. J. M. Dormans, D. J. Taylor, P. J. van Veldhoven, *J. Appl. Phys.* **1994**, *76*, 2405.
- [21] X. J. Lou, M. Zhang, S. A. T. Redfern, J. F. Scott, *Phys. Rev. Lett.* **2006**, *97*, 177601.
- [22] W. Warren, D. Dimos, B. Tuttle, R. Nasby, G. Pike, *Appl. Phys. Lett.* **1994**, *65*, 1018.
- [23] A. Gruverman, O. Auciello, H. Tokumoto, *Appl. Phys. Lett.* **1996**, *69*, 3191.
- [24] E. L. Colla, S. Hong, D. V. Taylor, A. K. Tagantsev, N. Setter, K. No, *Appl. Phys. Lett.* **1998**, *72*, 2763.
- [25] E. L. Colla, I. Stolichnov, P. E. Bradely, N. Setter, *Appl. Phys. Lett.* **2003**, *82*, 1604.
- [26] H. W. Jang, S. H. Baek, D. Ortiz, C. M. Folkman, C. B. Eom, Y. H. Chu, P. Shafer, R. Ramesh, V. Vaithyanathan, D. G. Schlom, *Appl. Phys. Lett.* **2008**, *92*, 062910.
- [27] S. M. Yang, J.-G. Yoon, T. W. Noh, *Curr. Appl. Phys.* **2011**, *11*, 1111.
- [28] A. Gruverman, A. Kholkin, *Rep. Prog. Phys.* **2006**, *69*, 2443.
- [29] N. Balke, I. Bdikin, S. V. Kalinin, A. L. Kholkin, *J. Am. Ceram. Soc.* **2009**, *92*, 1629.
- [30] D. J. Kim, J. Y. Jo, T. H. Kim, S. M. Yang, B. Chen, Y. S. Kim, T. W. Noh, *Appl. Phys. Lett.* **2007**, *91*, 132903.
- [31] S. M. Yang, J. Y. Jo, D. J. Kim, H. Sung, T. W. Noh, H. N. Lee, J.-G. Yoon, T. K. Song, *Appl. Phys. Lett.* **2008**, *92*, 252901.
- [32] T. H. Kim, S. H. Baek, S. M. Yang, S. Y. Jang, D. Ortiz, T. K. Song, J. S. Chung, C. B. Eom, T. W. Noh, J.-G. Yoon, *Appl. Phys. Lett.* **2009**, *95*, 262902.
- [33] S. M. Yang, J. W. Heo, H. N. Lee, T. K. Song, J. G. Yoon, *J. Korean Phys. Soc.* **2009**, *55*, 820.
- [34] S. Zhukov, Y. A. Genenko, O. Hirsch, J. Glaum, T. Granzow, H. von Seggern, *Phys. Rev. B* **2010**, *82*, 014109.
- [35] M. Dawber, K. M. Rabe, J. F. Scott, *Rev. Mod. Phys.* **2005**, *77*, 1083.
- [36] N. Balke, M. Gajek, A. K. Tagantsev, L. W. Martin, Y.-H. Chu, R. Ramesh, S. V. Kalinin, *Adv. Funct. Mater.* **2010**, *20*, 3466.
- [37] N. M. Murari, S. Hong, H. N. Lee, R. S. Katiyar, *Appl. Phys. Lett.* **2011**, *99*, 052904.
- [38] S. Jesse, B. J. Rodriguez, S. Choudhury, A. P. Baddorf, I. Vrejoiu, D. Hesse, M. Alexe, E. A. Eliseev, A. N. Morozovska, J. Zhang, L. Q. Chen, S. V. Kalinin, *Nat. Mater.* **2008**, *7*, 209.
- [39] S. Hong, E. L. Colla, E. Kim, D. V. Taylor, A. K. Tagantsev, P. Muralt, K. No, N. Setter, *J. Appl. Phys.* **1999**, *86*, 607.
- [40] Y. Ishibashi, Y. Takagi, *J. Phys. Soc. Jpn.* **1971**, *31*, 506.
- [41] Y. W. So, D. J. Kim, T. W. Noh, J.-G. Yoon, T. K. Song, *Appl. Phys. Lett.* **2005**, *86*, 092905.
- [42] I. Horcas, R. Fernandez, J. M. Gomez-Rodriguez, J. Colchero, J. Gomez-Herrero, A. M. Baro, *Rev. Sci. Instrum.* **2007**, *78*, 013705.